Nanotechnology and Nano-Interface Controlled Electronic Devices
Editors: M. Iwamoto, K. Kaneto and S. Mashiko

CHAPTER 9

Carrier transport behavior in OLED

Tatsuo Mori and Teruyoshi Mizutani

Department of Electrical Engineering, Graduate School of Engineering, Nagoya University, Furo-cho, Chikusa-ku, Nagoya 464-8603, Japan

1. Conducting organic materials

Organic materials have been regarded as insulating before the appearance of conductive polymers. The concept of "organic semiconductor" was revealed from the studies of π-conjugated polymers, that polyacethylene was discovered, and that the doping method was developed [1,2]. In addition, research fields such as organic functional materials and organic electronics are growing through the application of photosensitive materials (photoconduction materials) to electrophotography. However, it is very unstable state for an essentially neutral organic molecule to ionize by negatively or positively discharging as shown in Fig. 1. Since the unstable state leads to a degeneration reaction (oxidation), it was thought to be one of interference factors for the practical use of organic materials. Organic light-emitting diodes (OLEDs) reported by Tang and VanSlyke in 1987 [3] can

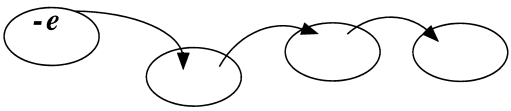

Fig. 1: The conception diagram of charge transfer in organic molecules.

be operated in the high-current region of > 1 A/cm^2 by means of the shielding of O_2 and H_2O.

2. Conduction in organic LED: experiment

The current–voltage (I–V) characteristics in OLEDs show a non-linear behavior. For example, Figs. 2 and 3 show the current density–luminance–voltage and luminance–current density characteristics of ITO/TPD[50nm]/Alq3[50nm]/AlLi and ITO/CuPc [30nm]/NPD[50nm]/Alq3[50nm]/LiF[0.6nm]/Al, respectively. ITO is indium-tin-oxide and a typical transparent electrode. TPD is *N*,*N*′-diphenyl-*N*,*N*′-bis(3-methylphenyl)-1,1′-diphenyl-4,4′-diamine and a famous but old-type hole transport material. Alq3 is 8-hydroxyquinoline aluminum (Alq3) and a most famous emitting material. CuPc is Phthalocyanine Copper as a hole injection layer. NPD is *N*,*N*′-di(1-naphthyl)-*N*,*N*′-diphenyl-1,1′-diphenyl-4,4′-diamine and a famous and high T_g (glass transition point) hole transport material. The fabrication process is shown in the previous paper [4–6].

Although the total thickness of a trilayer OLED is thicker than that of a bilayer OLED, both current densities are almost the same without increasing operating voltage. That is, electroluminescence is observed in the trilayer OLED at lower electric field. After the current shows Ohmic behavior below a few volts, the current increases steeply and shows non-linear behavior. However, as soon as EL, in other words, electron–hole

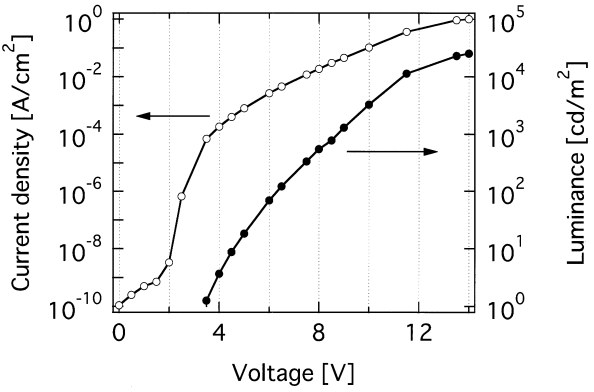

Fig. 2: The current density–luminance–voltage characteristics of ITO/TPD[50nm]/Alq3[50nm]/AlLi.

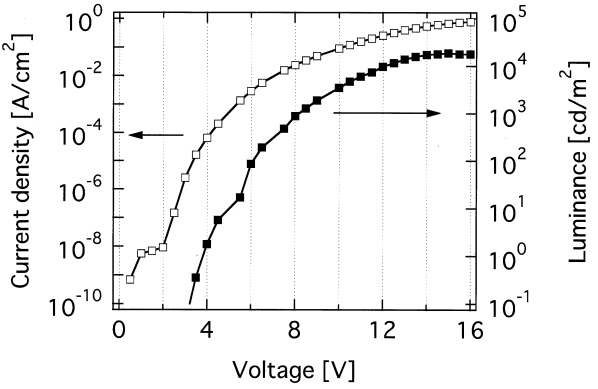

Fig. 3: The current density–luminance–voltage characteristics of ITO/CuPc[30nm]/NPD[50nm]/Alq3 [50nm]/LiF[0.6nm]/Al.

recombination can be observed, the current increases loosely and is proportional to V^4. Luminance is proportional to current density. We use these experimental data in the following discussion.

3. Conduction in organic LED: modeling

If the carrier conduction in a material is unipolar, its current density can be described as

$$J = qn\mu E, \tag{1}$$

where q is the charge, n is the carrier density, μ is the charge carrier mobility, and E is an electric field. However, if the current in a material is caused by many kinds of charged carriers (i.e. electron, hole, anions, cations), the current density must be described as

$$J = \sum_{i=1}^{k} q_i n_i \mu_i E, \tag{2}$$

where q_i is the charge of the ith carrier species, n_i is the carrier density of the ith carrier species, μ_i is the mobility of the ith carrier species, and E is an average electric field. Now we do not consider the modification of electric field in the layer.

Since most polymeric LEDs (PLEDs) consist of an additional hole injection layer and an emitting layer, it is physically consistent to apply Eq. 2 to their conduction. However, since organic low-molecular LEDs have multi function-separated layers, their conduction mechanism is very complicated.

Let us discuss the simple bilayer OLED with TPD as a hole transport layer and Alq3 as an emitting layer. TPD is well-known to be a hole transport material and then we consider only hole conduction in the TPD layer. In addition, the electron injection from Alq3 into TPD is strongly blocked because of the high barrier height between TPD and Alq3. On the other hand, Alq3 is a weak electron transport material because its electron

mobility is 100 times larger than its hole mobility [7]. Strictly speaking, the current of the TPD/Alq3 device must be written as

$$J = J_{\mathrm{TPD}} = J_{\mathrm{Alq3}} = J_{\mathrm{h,TPD}} + J_{\mathrm{e,TPD}} = J_{\mathrm{h,Alq3}} + J_{\mathrm{e,Alq3}}$$
$$= ep_{\mathrm{T}}\mu_{\mathrm{hT}}E_{\mathrm{T}} + en_{\mathrm{T}}\mu_{\mathrm{eT}}E_{\mathrm{T}} = ep_{\mathrm{A}}\mu_{\mathrm{hA}}E_{\mathrm{A}} + en_{\mathrm{A}}\mu_{\mathrm{eA}}E_{\mathrm{A}}, \quad (3)$$

where p and n are hole and electron densities, respectively. Subscripts T, A, e, and h mean TPD, Alq3, electron and hole, respectively. In a steady state, $J_{\mathrm{TPD}} = J_{\mathrm{Alq3}}$ (the law of continuity of current). Even if TPD thickness agrees with Alq3 thickness, the divided voltage of TPD layer is different from that of Alq3 because the former conductivity is lower than the latter. When the above experimental results are considered, $J_{\mathrm{e,TPD}}$ can be neglected. However, although hole mobility is smaller than electron mobility in Alq3, the third term on the right-hand side cannot be neglected because of the hole density injected from TPD. Consequently, Eq. 3 becomes

$$J = ep_{\mathrm{T}}\mu_{\mathrm{hT}}E_{\mathrm{T}} = ep_{\mathrm{A}}\mu_{\mathrm{hA}}E_{\mathrm{A}} + en_{\mathrm{A}}\mu_{\mathrm{eA}}E_{\mathrm{A}}. \quad (4)$$

The next problem is that carrier density and mobility in organic materials depend on electric field. That is, carrier density and mobility cannot be regarded as constant parameters. In addition, electric field is obtained as a function of position as well as each layer. As E_{T} or E_{A} is each average electric field in the TPD or Alq3 layer, this expression is ambiguous and it is right that the electric field should be described as $E(x)$. Of course, although the current also depends on time after applying voltage, $E(x)$ may be given as a distribution function of position since we treat the static state of the device. In addition, as high-performance OLEDs have a complicated multi-layer structure, one can understand that it is not easy to describe an analytical solution as the conduction model of OLEDs.

In OLEDs, the fact that organic materials have low carrier mobilities is thought to lead to that the conduction mechanism in OLEDs is due to the space charge limited current (SCLC) model. In PLEDs, the SCLC model is comparably easy to be accepted because their layer structures are simpler than those of low-molecular LEDs.

The conductive mechanism in OLEDs is categorized by two models: One is that the current in OLEDs is strongly controlled by injected carrier density since organic materials have low carrier concentration. The other is that it is strongly controlled by carrier mobility since organic materials have low carrier mobility. In the former example, some analyzed the current of OLED as Schottky current model controlled by hole or electron injection. However, the value of a physical parameter (a dielectric constant, the barrier height of carrier injection, etc.) determined from the approximate I–V curve is very different from that estimated from a direct measurement [8,9]. Although some interpretations for the conflict are suggested, they are not thought to be consistent with the physical phenomena. The carrier transport in OLEDs cannot be explained only by the unipolar carrier injection model.

4. Band model

In general, the conduction behavior in OLEDs is often explained using an energy diagram on the basis of the band model. For example, the OLEDs in Figs. 2 and 3 can

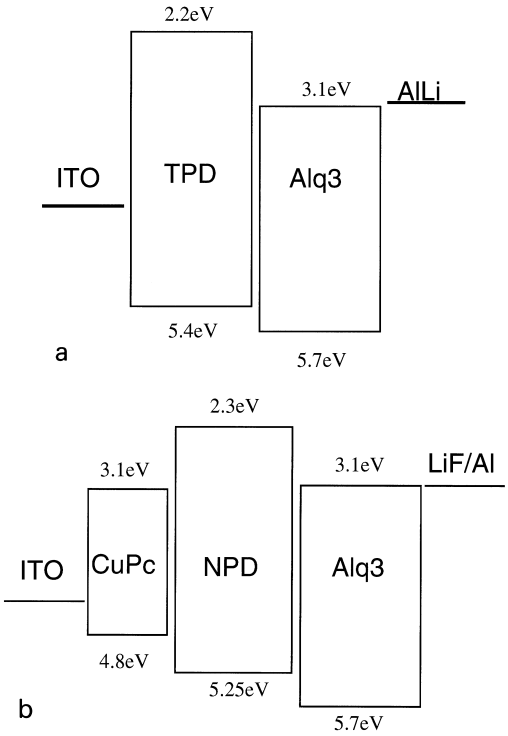

Fig. 4: (a) The energy diagram of ITO/TPD/Alq3/AlLi. (b) The energy diagram of ITO/CuPc/NPD/Alq3/LiF/Al.

be expressed by Fig. 4. When the energy diagram is made, the levels of the conduction band and valence band will be matched with LUMO (lowest unoccupied molecular orbital) and HOMO (highest occupied molecular orbital) levels, respectively. However, since the interaction between organic molecules is a van der Waals force, which is much weaker than covalent bond and metallic bond, the band width of the energy band becomes narrow even if an energy band may be formed in organic materials. The narrow band means low mobility for carrier transport in the band model. In nature, the carrier mobility in the band model is more than several hundreds $cm^2/V\,s$. The largest mobility in organic materials is at most 1 $cm^2/V\,s$, the carrier mobility in a pentacene crystal [10]. We must think that it is not appropriate to apply the band model to organic materials.

5. Hopping and tunneling models [11]

Let us remember that the carrier transport in organic materials is caused by alternate ionization between ionized molecules and neutral molecules, as shown in Fig. 1. That is,

$$M^{+(-)} + M \longrightarrow M + M^{+(-)}.$$

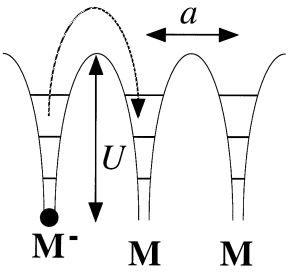

Fig. 5: The energy potential between molecules: a is molecular distance, U is potential energy.

The charge migration between molecules can be also explained by other, i.e. hopping and tunneling, processes.

Now we regard the potential diagram of neighboring molecules in Fig. 5. U is the barrier height of the potential. a is the distance between two neighboring molecules. The hopping probability of thermally activated charge is given by

$$P = \nu \exp\left(-\frac{U}{kT}\right), \tag{5}$$

where ν is trial frequency factor and k is Boltzmann constant. The mobility under electric field is given by the Einstein relation

$$\mu = \frac{eD}{kT}, \tag{6}$$

where D is the diffusion coefficient. In addition, using $D = Pa^2$, we obtain the following relation,

$$\mu = \frac{ea^2\nu}{kT} \exp\left(-\frac{U}{kT}\right). \tag{7}$$

When temperature increases, the preexponential factor decreases inversely proportional to temperature but the exponential term increases steeply. Consequently, the thermally activated hopping process has a positive temperature dependence.

On the other hand, the charge transfer between molecules may be caused by a tunneling process. The tunneling probability, P_T depends on the number of carriers colliding with the potential barrier, N and the tunneling factor, T. P_T can be described as the product of N and T, i.e. $P_T = NT$. T can be written as

$$T = T_0 \exp\left(-\frac{2w\sqrt{2m(U-E)}}{h}\right), \tag{8}$$

where T_0 is a constant, w is the barrier width, m is the electron mass, U is the barrier height of the potential barrier, E is the electron energy, and h is Planck's constant. Although the tunneling transfer due to the quantum mechanical mechanism is not affected by temperature, it strongly depends on the distance between one molecule and the counter as well as the electric field. Usually the effective distance for tunneling transfer is said to be < 1 nm.

6. Carrier injection model

Some researchers propose that the current in OLEDs can be simulated by the Schottky injection model [8,9]. The ground for their proposal is the temperature dependence of the current as shown in Fig. 6. If the current in OLEDs could be simulated by the tunneling injection model, it would not have shown a remarkable temperature dependence. However, let us remember Eq. 1. Since organic materials do not have intrinsic carrier density because they are essentially insulators, carrier density in bulk is due to carrier injection from the electrodes. Therefore, if current depended on only carrier density, we would consider the Schottky injection for the conduction in OLEDs since the current in OLEDs has temperature dependence. But we need to remember that the carrier transportation in organic materials is not caused by band conduction, but by such a discontinuous process as hopping conduction. The hopping conduction model has temperature dependence.

The current due to Schottky injection is described as

$$J = AT^2 \exp\left(\frac{\beta E^{1/2} - \phi}{kT}\right), \tag{10}$$

where A is Richardson–Dushman's constant, ϕ is the barrier height of carrier injection, and β is defined as

$$\beta = \sqrt{\frac{e^3}{4\pi\varepsilon}}. \tag{11}$$

This current depends on the squared electric field as well as temperature. In order to judge whether Schottky current can be applied to the conduction current of a material or not a Schottky-plot, $\ln J : E^{1/2}$, is often used. When the dielectric constant estimated from the gradient of the graph agrees with the experimental value, it is possible that the conduction mechanism in the material may be due to Schottky emission current. If the dielectric constant does not agree with the experimental one, we think that the conduction mechanism should be treated carefully.

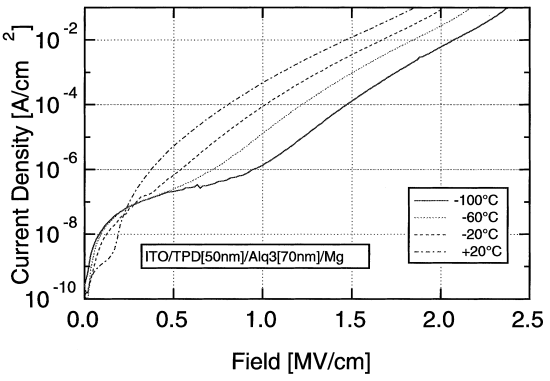

Fig. 6: The temperature dependence of the current density–electric field characteristics of ITO/TPD[50nm]/Alq3[70nm]/Mg.

7. Space Charge Limited Current (SCLC)

7.1. Theoretical introduction

Although SCLC is the conduction model controlling carrier injection, it is not an injection-controlled conduction but a bulk-controlled one. Some researchers believe that the current density, J, due to SCLC equation is

$$J = \frac{9}{8}\frac{\varepsilon\mu V^2}{d^3}, \tag{12}$$

where e is a quantum of electricity, μ is the mobility of carriers, V is an applied voltage, and d is the sample thickness.

However, this equation is a special solution obtained from an original Poisson equation and the boundary condition, $E(0) = 0$, $V(0) = 0$. In this section, we discuss the problem of the SCLC model.

The SCLC model ought essentially to be applied to unipolar conduction. When voltage is applied to an insulator (organic material) interposed by two electrodes and the charged carriers injected from an electrode are not neutralized by the counter charged carriers injected from the counter electrode, the injected charged carriers form a space charge around the electrode. This space charge modifies the electric field between the electrodes in the case of low mobility. The homo space charge accumulated in front of an electrode reduces the electric field on the electrode. Therefore, the carrier injection after forming the space charge strongly depends on the modified electric field due to space charge.

The necessary conditions that a conduction current becomes a SCLC are the following:

1. the current due to injected carriers has the same or higher value as the Ohmic current;

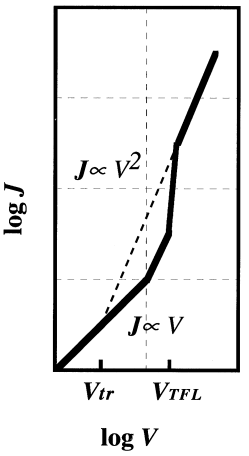

Fig. 7: Typical SCLC characteristics.

2. the dielectric relaxation time of the material is longer than the carrier drift time between the electrodes in the material.

A typical SCLC example is the anode current–voltage characteristics of a two-electrode vacuum tube. In general, it is not easy for organic materials to satisfy the necessary condition 1.

Let us find Eq. 12 from Poisson's equation. We regard a one-dimensional system containing the sample with two electrodes. The interface between cathode and sample is $x = 0$. Now we imagine that electrons are injected into the sample. Poisson's equation is

$$\frac{\mathrm{d}^2\varphi}{\mathrm{d}x^2} = -\frac{en}{\varepsilon}, \tag{13}$$

where φ is the potential in the sample, n is injected electron density, and ε is the dielectric constant of the sample. The current density, J in the sample is described as

$$J = en\mu E, \tag{14}$$

where μ is the electron mobility and E $(= -\mathrm{d}\varphi/\mathrm{d}x)$ is electric field in the sample. Deleting n using the two equations 13 and 14,

$$\frac{\mathrm{d}E}{\mathrm{d}x} = \frac{J}{\varepsilon\mu E}. \tag{15}$$

Integrating Eq. 15 with respect to x after separating variables,

$$E^2(x) = \frac{2J}{\varepsilon\mu}x + C, \tag{16}$$

Using $E(0) = 0$, $C = 0$, therefore:

$$E(x) = \pm\sqrt{\frac{2J}{\varepsilon\mu}}x^{1/2}. \tag{17}$$

However, as the positive solution is not appropriate for this case,

$$E(x) = -\sqrt{\frac{2J}{\varepsilon\mu}}x^{1/2}. \tag{18}$$

$V(x)$ is given by integrating $E(x)$ with respect to x.

$$\begin{aligned} V(x) &= -\int_0^x E(x)\,\mathrm{d}x = \int_0^x \sqrt{\frac{2J}{\varepsilon\mu}}x^{1/2}\,\mathrm{d}x \\ &= \sqrt{\frac{8J}{9\varepsilon\mu}}x^{3/2} + C' \end{aligned} \tag{19}$$

We can use $V(0) = 0$, $C' = 0$. When the sample thickness is d and the applied voltage is V, the following equation can be given (Fig. 8),

$$J = \frac{9}{8}\frac{\varepsilon\mu V^2}{d^3}. \tag{12}$$

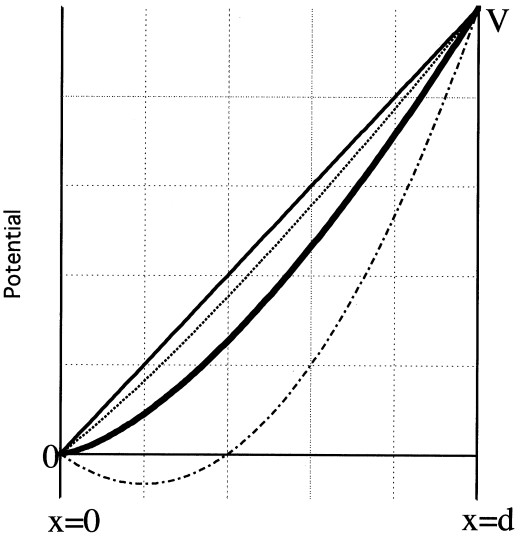

Fig. 8: The potential distribution between cathode and anode: thin solid line means average electric field. Thick solid line is the potential on the equilibrium condition.

7.2. Experimental verification [13]

There are many papers using the SCLC model [14–18]. In our opinion, there are some problems for applying the SCLC model to organic LEDs. The system of the organic LED may not satisfy the above necessary conditions.

Fig. 9 shows the experimental and calculated J–V characteristics of the OLEDs as shown in Figs. 2 and 3. The lines with marker are the experimental curves and the lines without marker are calculated curves. Estimated values are used for the parameters: $\varepsilon = \varepsilon_r \varepsilon_0$, the dielectric constant of organic material, ε_r is about 3 and ε_0 is the permittivity of vacuum, μ is 10^{-3}–10^{-6} $\mathrm{cm}^2/\mathrm{V\,s}$. The thickness, d, is the sum of the CuPc and NPD layers in the dash-dotted line. d is the total thickness of organic layers for the other lines. The carrier mobility in both the dash-dotted line and the solid line is 10^{-3} $\mathrm{cm}^2/\mathrm{V\,s}$. That of dotted line, short-dashed one, and long-dashed one is 10^{-4}, 10^{-5}, and 10^{-6} $\mathrm{cm}^2/\mathrm{V\,s}$, respectively.

In the low current region, the experimental current behavior does not agree with the calculated curves. In the high current region, the value of the former approaches the calculated one. A decrease of effective thickness contributes to an increase of current. Since the carrier mobility estimated by the TOF method is caused by the carrier transfer due to photoexcited carriers with high energy (> 3 eV), it is possible to overestimate the intrinsic mobility which will be excited by thermal activation ($\sim$0.026 eV). Carrier mobility of organic materials needs to be discussed in detail.

Fig. 10 shows the conductivity, dielectric relaxation time and drift time–voltage characteristics of ITO/TPD[50nm]/Alq3[50nm]/AlLi. Each parameter is calculated by the following. The apparent conductivity, σ is calculated by $\sigma = J/E = Jd/V$. The

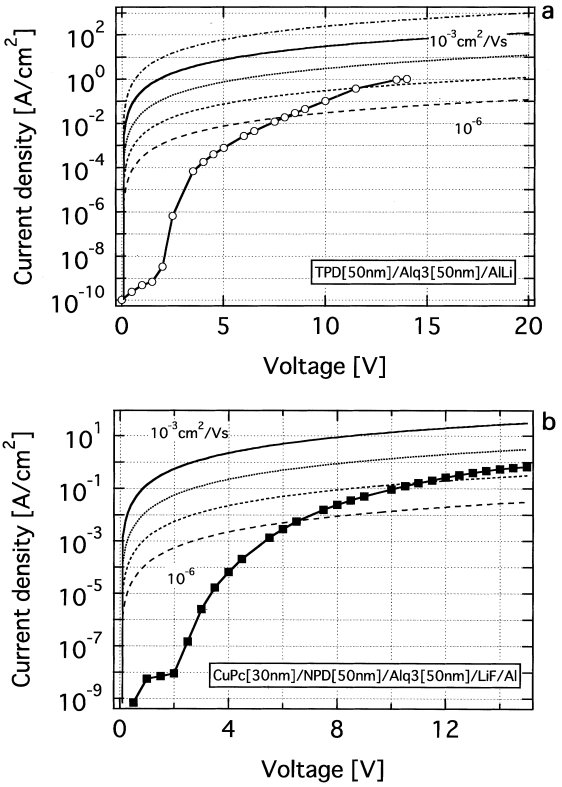

Fig. 9: The current density–voltage characteristics of ITO/TPD/Alq3/AlLi (a) and ITO/CuPc/NPD/Alq3/LiF/Al (b). The lines with marker are the experimental curves and the lines without marker are calculated curves. TPD thickness is used as d in the dash-dotted line. d is the total thickness of organic layers in the other lines. The carrier mobility in both the dash-dotted line and solid line is 10^{-3} cm^2/V s. That of the dotted line, short-dashed one, and long-dashed one is 10^{-4}, 10^{-5}, and 10^{-6} cm^2/V s, respectively.

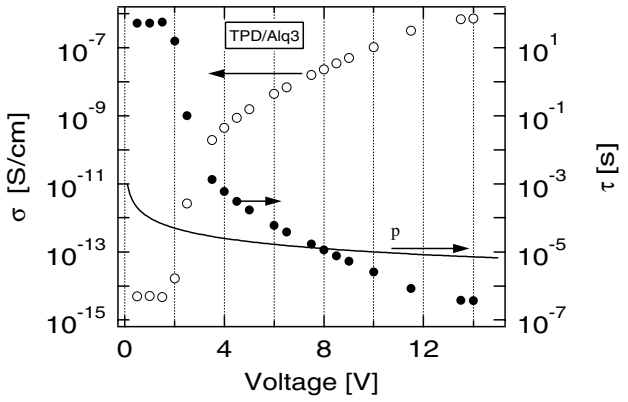

Fig. 10: The apparent conductivity, dielectric relaxation time and drift time as function of voltage in ITO/TPD/Alq3/AlLi: closed circles mean apparent conductivity, open circles mean dielectric relaxation time, and solid line is calculated drift time.

dielectric relaxation time, τ, is estimated from $\tau = \varepsilon/\sigma$. We used $3\varepsilon_0$ as the dielectric constant of organic materials: ε_0 is the permittivity of vacuum. The drift time, t_d is calculated by $t_d = d/v = d/\mu E$. We used a constant mobility, 10^{-6} cm^2/V s, as average mobility. The hole mobility in TPD was estimated to be $\sim 10^{-3}$ cm^2/V s [19] and the hole and electron mobilities in Alq3 were estimated to be $\sim 10^{-5}$ and $\sim 10^{-7}$ cm^2/V s [7], respectively. Since these values were obtained by the time-of-flight method, we think that the carrier mobility obtained by the time-of-flight method is overestimated as the carrier mobility of organic material. In addition, the exact drift time in organic LEDs can be obtained by summing the hole drift time in TPD and the electron drift time in Alq3. However, such a calculation process is not consistent with the SCLC model. Therefore, we used a lower value as average mobility.

The apparent conductivity of ITO/TPD/Alq3/AlLi is almost constant, $\sim 10^{-14}$ S/cm below ~ 2 V. It increases steeply with starting carrier injection and achieves to $\sim 10^{-6}$ S/cm. Consequently the dielectric relaxation time is lower than the average drift time. Therefore, we conclude that the necessary condition 2 for the SCLC model is not satisfied in OLEDs. We have to consider the conduction mechanism in OLEDs on the basis of real charge transfer between molecules.

8. Simulation of carrier transport by directly calculated hopping model [20–26]

8.1. Introduction

Although the structure of OLEDs in which organic layers are sandwiched between two electrodes is simple, the light-emitting mechanisms of the device are quite complicated. These mechanisms may be roughly divided into three processes: the carrier injection process from each electrode, the carrier transport process, and the emission process via excitons generated by electron–hole recombination. For example, many researchers tried to explain the carrier injection mechanism of OLED from the viewpoint of experimental current–voltage characteristics. However, such external information is insufficient to explain the injection mechanism. Clarification of each process will ease improvement of current performance of the device.

When we improve on the device performance, it is important to discuss the balance between electron and hole injections. Rate of electron–hole recombination, electric field, and space-charge distributions in the OLED are also important. However, it is impossible to obtain and evaluate these parameters experimentally because these parameters are "internal" OLED parameters. In the present work, we assumed a simple model and attempted to calculate carrier behavior in OLED in order to clarify light-emitting mechanisms.

Many groups have attempted to simulate I–V characteristics of devices [27–35]. Calculations were carried out using a "continuous model" in which conduction current density is explained by carrier drift and carrier diffusion.

Considering recombination and Fowler–Nordheim injection, Khramtchekov et al. showed the distributions of electric field and current flows in a bilayer OLED [27]. Davids et al. assumed that initial hole distribution followed Maxwell–Boltzmann statistics as accompanied with Schottky and tunneling injection [28].

Crone et al. estimated the distributions of electric field, hole and electron currents, and recombination rate [29]. Although they explained the values by the conduction mechanism due to the SCLC model, they pointed out that space charge is not significant. Kawabe et al. analyzed the conduction characteristics in PLEDs on the basis of semiconductors [30]. They used Fowler–Nordheim and SCLC currents.

Malliaras et al. used numerical methods to calculate the current and the efficiency of a single-layer organic LED, taking into account field-dependent mobilities, diffusion, and thermionic injection [31]. Staudigel et al. quantitatively simulated the conduction and EL mechanism in multi-layer OLEDs by a one-dimensional numerical model [32]. Of course, they compared the experimental results with their simulated data.

Crone et al. gave the carrier mobility of a single-layer PLED the field dependence of the Pool–Frenkel form [33]. And they treated the conduction of PLEDs as a bipolar mechanism. They tried to explain the change of conduction in a single-layer PLED caused by the difference of cathode metal using their model. They claimed that their model successfully describes the I–V characteristics of a single-layer PLED. Crone et al. applied their conduction model to single-layer OLEDs [34]. They calculated the spatial variation of the carrier densities, electric field, and recombination rate. Tutis et al. proposed the discrete carrier injection model due to tunneling injection [35]. (However, some equations in this paper have errors!)

Tsutsui et al. pointed out that the main factor of current in organic film is not always an equilibrium carrier density [36]. In general, space charge limited current (SCLC) is used to explain conduction of organic thin films such as OLEDs. In this model, the injection field becomes zero, so that carrier density is infinite at the interface. However, this density never becomes infinite since sites are limited in organic films.

8.2. Model in detail

We proposed a one-dimensional discontinuous model for simulation as shown in Fig. 11. Simulation of carrier behavior in an insulator is based on the hopping model proposed by Iwamoto and Hino [37]. Although carrier density is not limited in continuous models, the carrier number accepted by a molecule is limited in our model. Because the carrier transport between organic molecules is regarded as an intermolecular oxidation–reduction, our model approximates carrier behavior more accurately than conventional continuous models. In continuous models, the carrier number accepted by a molecule is not limited.

We assumed a bilayer OLED of ITO/TPD/Alq3/Al. Thickness of each organic layer is 50 nm. Since an Alq3 molecule is represented by a sphere of 0.8 nm diameter, we approximate that these molecules are arranged with average distance of 1.73 nm in an electric field. The number of sites is 30. Molecular stacking is not considered. Maximum carrier density per unit area is 10^{18} m^{-2} [$(10^9)^2$].

Most parameters obtained by experiments can be found in our previous papers [20–26]. The carrier conduction process is assumed as follows: (I) a molecule is a hopping site, (II) a site can be occupied by an electron or a hole at most, (III) carriers move only to adjacent sites, and (IV) the hopping rate depends on not only to carrier density, but also to the rate of unoccupied adjacent sites. Conduction currents from the kth site to the

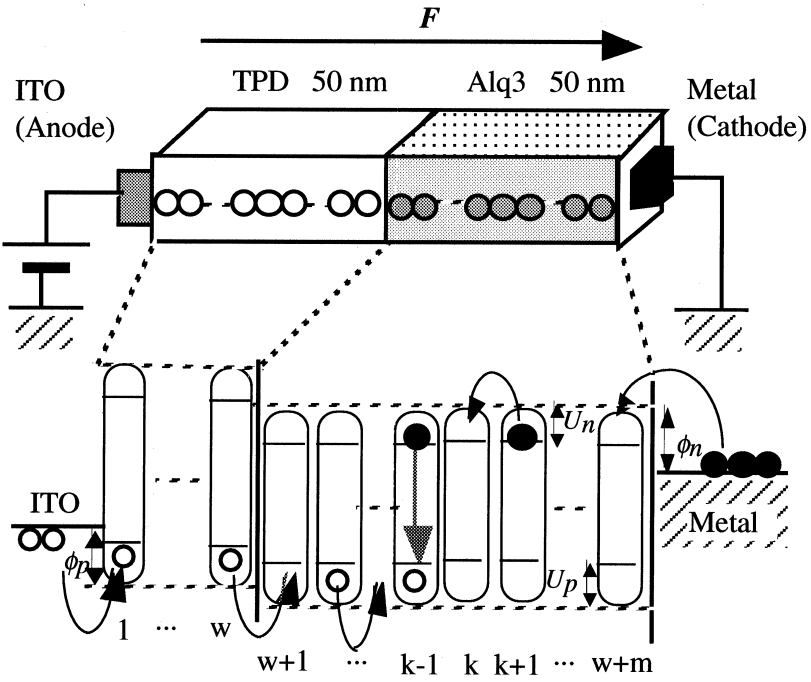

Fig. 11: Diagram of the one-dimensional hopping model.

adjacent $k+1$th site for holes ($J_{p(k,k+1)}$) are represented as

$$J_{p(k,k+1)} = \nu'_p q p_k \left[\frac{N - p_{k+1} - r_{k+1}}{N}\right] \exp\left(\frac{qaF_{(k,k+1)}}{2k_B T}\right) - \nu'_p q p_{k+1} \left[\frac{N - p_k - r_k}{N}\right] \exp\left(\frac{-qaF_{(k,k+1)}}{2k_B T}\right)$$
$$(k = 1,2,\ldots,m) \tag{20}$$

$$\nu'_p = \nu \exp\left(\frac{-U'_p}{k_B T}\right) , \tag{21}$$

and those for electrons ($J_{n(k,k+1)}$) are

$$J_{n(k,k+1)} = \nu'_n q n_k \left[\frac{N - n_{k+1} - r_{k+1}}{N}\right] \exp\left(\frac{qaF_{(k,k+1)}}{2k_B T}\right) - \nu'_n q n_{k+1} \left[\frac{N - n_k - r_k}{N}\right] \exp\left(\frac{-qaF_{(k,k+1)}}{2k_B T}\right)$$
$$(k = 1,2,\ldots,m-1) \tag{22}$$

$$\nu'_n = \nu \exp\left(\frac{-U'_n}{k_B T}\right), \tag{23}$$

where N represents the maximum site density for a molecular layer ($= 10^{18}$ m^{-2}); p_k, n_k, and r_k (m^{-2}) are densities of the hole, electron, and exciton of the kth site, respectively; $(k,k+1)$ is an electric field between the kth and $(k+1)$th site; and U_p' and U_n' (eV) are hopping barriers for holes and electrons, respectively. Also, ν (s^{-1}) is the attempt-to-escape frequency; m shows site numbers for Alq3; and T, k_B, and q are temperature, the Boltzmann constant, and elementary charge, respectively. The hopping distance a is assumed to be 1.73 nm, which is the average distance between the two centers of adjacent molecules. U_p and U_n were calculated using the equation for conventional hopping transport from experimental carrier mobility, μ_p and μ_n [7]. Electron mobility is about 100 times higher than hole mobility in Alq3; hole mobility in the TPD bulk is about five orders of magnitude higher than that in the Alq3 bulk. We use U_p (0.27 eV) as U_p' and U_n (0.15 eV) as U_n', respectively, in Alq3. At the TPD/Alq3 interface, U_p' and U_n' are $U_p + \phi_{bp}$ and $U_n + \phi_{bn}$, where ϕ_{bp} (0.26 eV) and ϕ_{bn} (0.83 eV) are barrier heights for the hole and the electron, respectively. Since ϕ_{bn} is so high that electrons are almost blocked at the TPD/Alq3 interface, electron behavior can be ignored in the TPD bulk. We use both Schottky emission and Fowler–Nordheim emission for electron injection from the cathode. The electron current density passing between the Alq3 and the cathode interface, $J_{n(m,m+1)}$, is assumed as

$$J_{n(m,m+1)} = \left[\frac{N - n_m - r_m}{N}\right]\left[A_n T^2 \exp\left(\frac{-\phi_n}{k_\mathrm{B}T}\right)\exp\left(\frac{q}{k_\mathrm{B}T}\sqrt{\frac{qF_{(m,m+1)}}{4\pi\varepsilon_\mathrm{r}\varepsilon_0}}\right) + \rho\frac{qF_{(m,m+1)}^2}{8\pi h\phi_n}\exp\left(\frac{-8\pi\sqrt{2m^*\phi_n^3}}{3qhF_{(m,m+1)}}\right)\right] - \nu_n' q n_m \exp\left(\frac{-qaF_{(m,m+1)}}{2k_\mathrm{B}T}\right), \quad (24)$$

where ϕ_n (eV) is the barrier height for electron injection from the cathode to an Alq3 molecule and is estimated to be 0.67 eV, and A_n, ε_0, and ε_r are initial parameters based on the Richardson–Dushman constant for electrons, vacuum permittivity, and dielectric constant of Alq3 bulk, respectively. Hole injection from an anode is assumed to be due to Schottky emission. The hole current density passing through the TPD/Alq3 interface, $J_{p(0,1)}$, is assumed to be the same at the ITO/TPD interface because the space charge density is negligible in the TPD bulk except for the site adjacent to the Alq3. Thus, the interface is assumed to be a hole reservoir as shown in Eq. 25. As holes are accumulated in the TPD site closest to the TPD/Alq3 interface, we can regard this site as a reservoir for holes. Hole density is represented as p_res, that is, $p_0 = p_\mathrm{res}$. Therefore, the hole conduction current passing through the TPD/Alq3 interface is obtained by substituting p_res into Eq. 20:

$$J_{p(0,1)}) = \left[\frac{N - p_\mathrm{res}}{N}\right] A_p T^2 \exp\left(\frac{-\phi_p}{k_\mathrm{B}T}\right)\exp\left(\frac{q}{k_\mathrm{B}T}\sqrt{\frac{qF_{(0,1)}}{4\pi\varepsilon_\mathrm{r}\varepsilon_0}}\right) - \nu_p' q p_1 \left[\frac{N - p_\mathrm{res}}{N}\right]\exp\left(\frac{-qaF_{(0,1)}}{2k_\mathrm{B}T}\right). \quad (25)$$

The barrier height, ϕ_{bp}, for hole injection from the TPD molecule to Alq3 is estimated to be 0.26 eV. Current density flowing in an external circuit consists of the

hole conduction component Eq. 26 and the electron conduction one Eq. 27, both of which are derived from the continuity equation under DC field, J_p is hole current density; $J_{p(0,1)}$, $J_{p(m,m+1)}$, $wJ_{p(0,1)}$ and the sum of $J_{p(k,k+1)}$ are hole current densities flowing in the TPD/Alq3 interface, the Alq3/Al interface, the TPD bulk, and the Alq3 bulk, respectively.

$$J_p = \frac{1}{2}\{J_{p(0,1)} + J_{p(m,m+1)}\} + wJ_{p(0,1)} + \sum_{k=1}^{m-1}\{J_{p(k,k+1)}\}. \tag{26}$$

In the equation above, J_n is electron current density; $J_{n(0,1)}$, $J_{n(m,m+1)}$, and the sum of $J_{n(k,k+1)}$ are flowing the TPD/Alq3 interface, the Alq3/Al interface, and the Alq3 bulk. Electron mobility in the TPD bulk is very low and electron current is negligible.

$$J_n = \frac{1}{2}\{J_{n(0,1)} + J_{n(m,m+1)}\} + \sum_{k=1}^{m-1}\{J_{n(k,k+1)}\}. \tag{27}$$

Here, w is the number of sites in TPD. Time variation of hole density is shown in Eq. 28 and that of electron density is shown in Eq. 29.

$$\frac{\mathrm{d}p_k}{\mathrm{d}t} = \frac{1}{q}\{-J_{p(k,k+1)} + J_{p(k-1,k)}\} - Rn_k p_k, \tag{28}$$

$$\frac{\mathrm{d}n_k}{\mathrm{d}t} = \frac{-1}{q}\{-J_{n(k,k+1)} + J_{n(k-1,k)}\} - Rn_k p_k, \tag{29}$$

where R is the electron–hole recombination coefficient for Alq3 molecules. The fields are expressed as Eqs. 30–32, which are derived from the Poisson equation.

$$F_{(k,k+1)} = \frac{-qa}{\varepsilon_r\varepsilon_0 d}\left[\sum_{s=1}^{k}\left(s-\frac{1}{2}\right)(p_s - n_s)\right] + \frac{qa}{\varepsilon_r\varepsilon_0 d}\left[\sum_{s=k+1}^{m}\left(m-s+\frac{1}{2}\right)(p_s - n_s)\right] - \frac{V_a}{d}, \tag{30}$$

$$F_{(0,1)} = \frac{-qa}{\varepsilon_r\varepsilon_0 d}\left[\sum_{s=k+1}^{m}\left(m-s+\frac{1}{2}\right)(p_s - n_s)\right] - \frac{V_a}{d}, \tag{31}$$

$$F_{(m,m+1)} = \frac{-2qa}{\varepsilon_r\varepsilon_0 d}\left[\sum_{s=k+1}^{m}\left(m-s+\frac{1}{2}\right)(p_s - n_s)\right] - \frac{V_a}{d}. \tag{32}$$

In these equations, d and V_a are thickness and applied voltage of the device. When L is the length of exciton diffusion and τ is the fluorescence lifetime in Alq3, the diffusion coefficient, D, is shown by

$$D = \frac{L^2}{\tau}. \tag{33}$$

Time variation of exciton density is shown by

$$\frac{\mathrm{d}n_k}{\mathrm{d}t} = Rn_k p_k + D(N - p_k - n_k - r_k)\frac{\mathrm{d}^2 r_k}{\mathrm{d}k^2} + Dr_k\frac{\mathrm{d}^2}{\mathrm{d}k^2}(N - p_k - n_k - r_k) - \frac{r_k}{\tau}. \tag{34}$$

Electroluminescence (EL) intensity is assumed to be proportional to the sum of $Rn_k p_k$ in the Alq3 layer (k: from 1 to m),

$$\mathrm{EL} \propto \frac{1}{\tau} \sum_{k=1}^{m} Rn_k p_k. \tag{35}$$

8.3. Carrier behaviors

In this simulation, the carrier (electron and hole) distribution and field distribution as well as current density and EL intensity are calculated when a DC step voltage is applied.

Distributions of hole density, electron density, and exciton generation density are shown in Figs. 12, 13, amd 14, respectively. In these calculations, a recombination rate $R = 1.0 \times 10^{-5}$ m^2/s is used to calculate the exciton generation distribution.

Holes are accumulated near the TPD/Alq3 interface, as shown in Fig. 13. Hole density decreases with distance from the TPD/Alq3 interface. Holes are accumulated within 10 nm distance from the interface (Fig. 12) because of the low hole mobility in the Alq3 layer. In the emission layer (Alq3), electrons injected from a cathode move to the TPD/Alq3 interface. Electrons are comparatively uniformly distributed in Alq3 bulk (10 nm $\leq$ position $\leq$ 50 nm), and decrease near the TPD/Alq3 interface. Electron density near the TPD/Alq3 interface is lower than that near the cathode, as shown in Fig. 13. Distribution of hole density differs from that of electron density because the electron mobility is 100 times faster than the hole mobility in the Alq3 layer. Fig. 14 shows distribution of generated exciton density after 30, 100, and 250 ns. Exciton generation due to recombination occurs near the TPD/Alq3 interface. Distribution of exciton generation depends on the product of hole and electron densities. The electron density rapidly decreases near the interface because of the recombination of electrons and holes, resulting in generating excitons near the TPD/Alq3 interface.

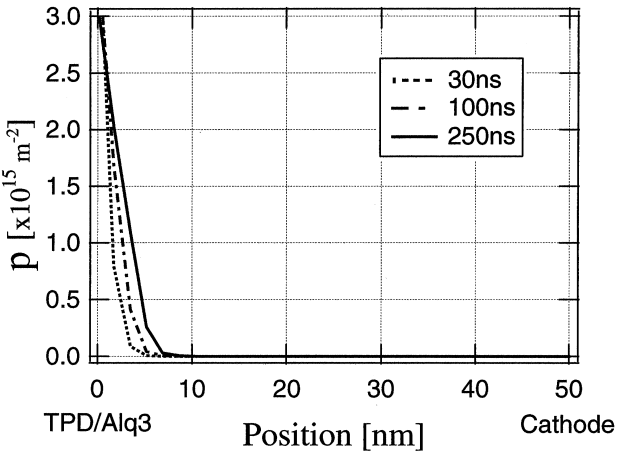

Fig. 12: Distribution of hole density in Alq3 layer.

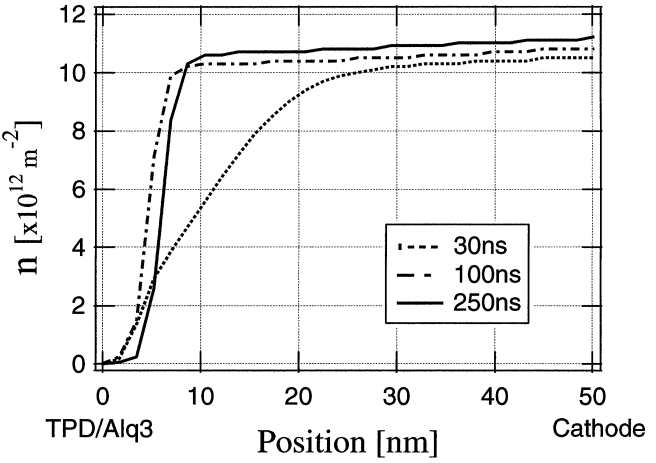

Fig. 13: Distribution of electron density in Alq3 layer.

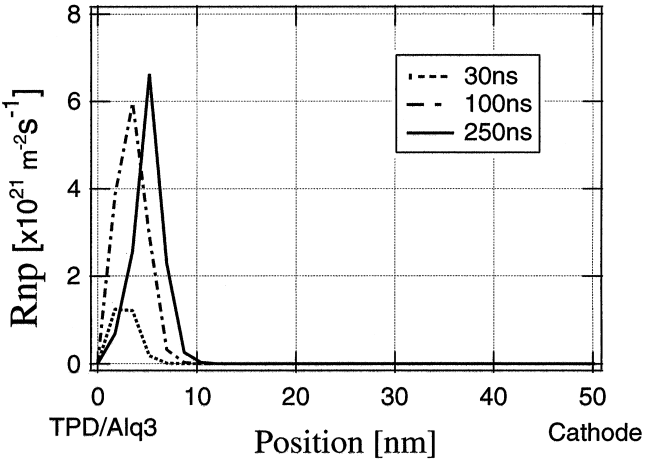

Fig. 14: Distribution of generated exciton density in Alq3 layer.

Exciton generation density achieves a maximum value and it moves from the interface with time. Since electron density is lower than hole density, all electrons are considered to recombine with holes before reaching the TPD/Alq3 interface.

Fig. 15 shows the field distribution in both organic layers at an average field of $F_a = 140$ MV/m. Field distortion in TPD bulk is little observed at $F_a = 140$ MV/m where an OLED shows strong luminance of over 600 cd/m^2. Our one-dimensional discontinuous calculation model suggests that conduction in OLEDs cannot be explained by a typical SCLC conduction model since field distortion is not observed near both cathodes in organic layers.

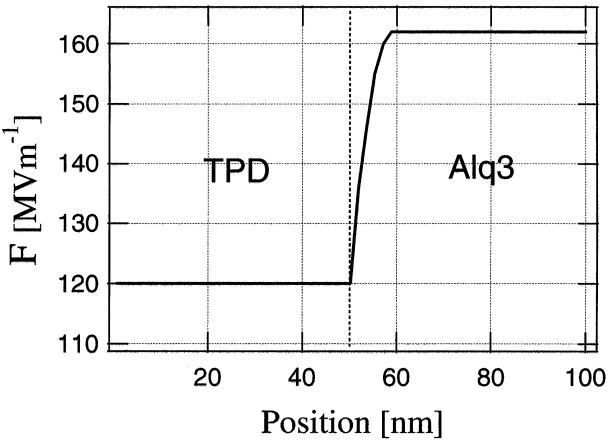

Fig. 15: Distribution of electric field at an average field of 140 MV/m.

8.4. Transient response characteristics

Figs. 16 and 17 show calculated time dependence of current density and EL intensity at $F_a = 140$ MV/m. The hole current density, J_p, at 100 ns decreases until it reaches 90% at 30 ns. Since distribution of hole density spreads into the Alq3 bulk over time, as shown in Fig. 12, accumulation of electrons results in inducing field relaxation near the interface (Fig. 15). Also, the amount of injected electrons decreases. At 30 ns, the electron current density is 90% of that at 100 ns and saturated. Thus, electron current density appears to be saturated after 100 ns. It has a turning point at 30 ns; after which EL begins to increase. Amounts of injected electrons and recombining electrons

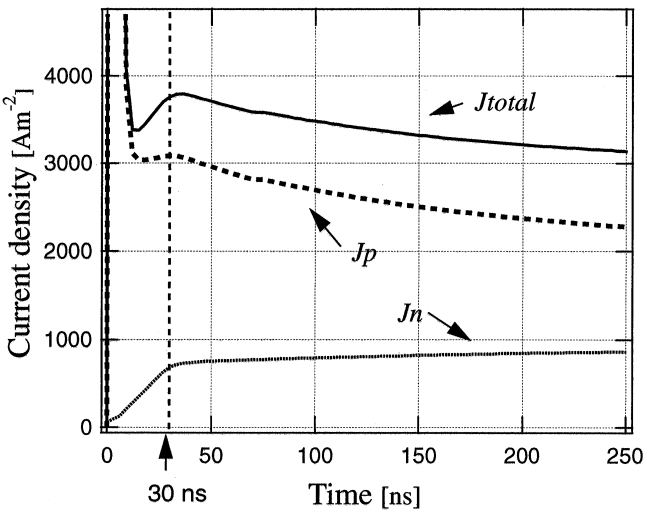

Fig. 16: Time dependence of current densities at an average field of 140 MV/m.

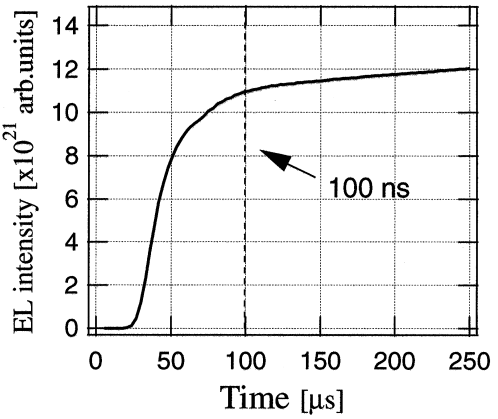

Fig. 17: Time dependence of EL intensity at an average field of 140 MV/m.

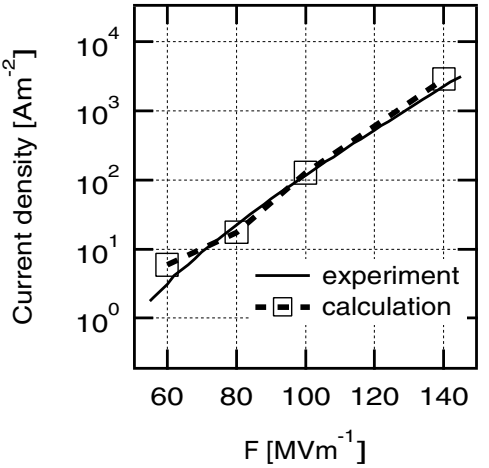

Fig. 18: Comparison of calculated and experimental field dependence of current density.

equalize due to exciton generation near the TPD/Alq3 interface. When the applied electric field is small, ($F_a = 100$ MV/m), the delay time of EL (solid line) and 90% of EL value at 250 ns (dashed line) is longer than when a high electric field is applied.

Fig. 18 shows the calculated current densities flowing in an external circuit. The calculated current density normalized by the current density at $F_a = 100$ MV/m are used to calculate those at other F_a. The calculated curves (solid line) agree to the experimental ones (dashed line), as shown in Fig. 18. In our previous work, we considered only Schottky emission as electron injection mechanism. EL intensity (Fig. 19) did not agree with experimental values at low electric field, although the calculated density agreed with experimental data. Considering both Fowler–Nordheim emission and Schottky emission into the electron injection mechanism, Fowler–Nordheim emission is dominant in high fields, as shown in Fig. 20.

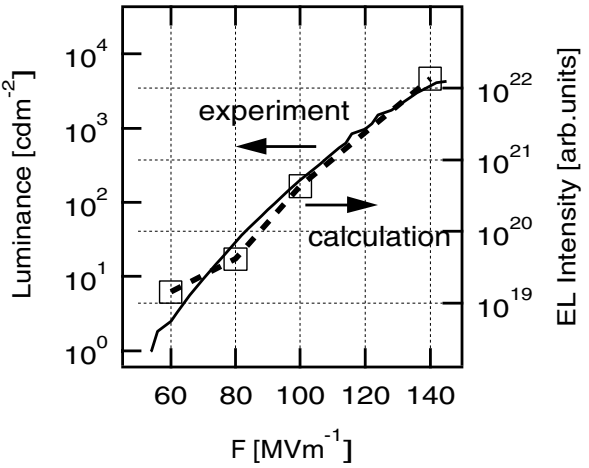

Fig. 19: Comparison of calculated and experimental field dependence of EL intensity.

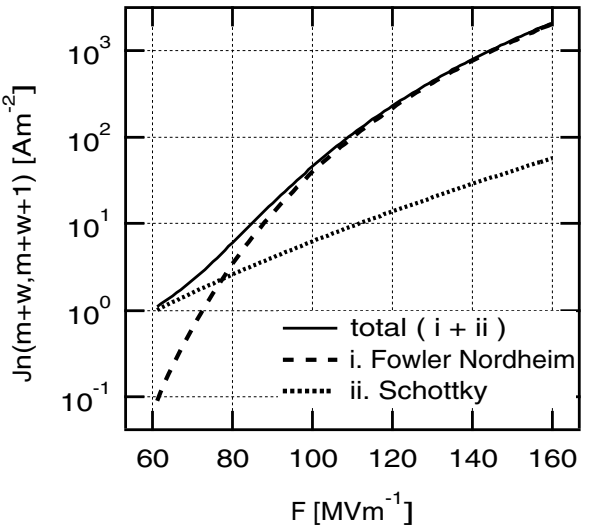

Fig. 20: Field dependence of electron injection.

8.5. Summary of the simulation

We assume a one-dimensional hopping conduction model for the OLED: each emitting molecule corresponds to a hopping site simulating actual charge transfer between adjacent molecules. Time dependence of carrier, exciton and EL intensity, and distributions of field and carrier density are calculated.

Hole and electron densities decrease near the TPD/Alq3 interface. As a result, the density of exciton generation achieves its maximum within 10 nm from the TPD/Alq3 interface. Field distribution due to the space charge effect is not apparent in the TPD

bulk. These results suggest that the conduction mechanism in bilayer OLEDs cannot be explained by a typical SCLC conduction model. This model accommodates Fowler–Nordheim emission as an electron injection mechanism. As a result, behavior of current density and EL intensity agree with measured current density and luminance. From above results, a simple bilayer and discontinuous model is effective for investigating OLED carrier behavior.

9. Conclusion

We showed that it is difficult to directly apply the SCLC model to OLEDs. If a researcher believes that the conduction mechanism of a material can be explained by a particular mechanism, that is, an equation, he can analyze the conduction current by the equation. And he may obtain the various information on the conduction mechanism of a material. However, if he does not verify his calculated parameters by means of other experimental results, his analysis will be almost nonsense in the special case with additional assumptions. Of course, our simulation is still incomplete and also needs to reflect the experimental results. Since OLEDs have multi-layer structure and a bipolar conduction mechanism, we have to treat the complicated conduction discretely.

References

1. H. Shirakawa, T. Ito, and S. Ikeda, Polym. J. **2**, 231 (1971).
2. M. Hirooka and T. Doi, Synthetic Metals **17** 372 (1987).
3. C.W. Tang and S.A. Vanslyke, Appl. Phys. Lett. **51** 913 (1987).
4. T. Mori, K. Imaizumi, K. Yamashita, T. Mizutani, and H. Miyazaki, Synthetic Metals **111–112** 79 (2000).
5. T. Mori, K. Obata, and T. Mizutani, J. Phys. D **32** 1198 (1999).
6. T. Kato, T. Mori, and T. Mizutani, Thin Solid Films **393** 109 (2001).
7. R.G. Kepler, P.M. Besson, S.J. Jacobs, R.A. Anderson, M.B. Sinclair, V.S. Valencia, and P.A. Cahill, Appl. Phys. Lett. **66** 3618 (1995).
8. E.g., J. Kalinowski, M. Cocchi, V. Fattori, and P.D. Marco, J. Phys. D **34** 2274 (2001).
9. M. Matsuura, T. Akai, M. Saito, and T. Kimura, J. Appl. Phys. **79** 264 (1996).
10. S. Naka, H. Okada, and H. Onnagawa, Synthetic Metal **91** 129 (1997).
11. S.F. Nelson, Y.Y. Lin, D.J. Gundlach, and T.N. Jackson, Appl. Phys. Lett. **72** 1854 (1998).
12. K. Yamashita and A. Kitani, *Dodensei-Yukihakumaku no Kinou to Sekkei (Function and Design of Conductive Organic Thin Films)*, (Kyoritsu Shuppan, Tokyo, 1998), pp. 18–25 [in Japanese].
13. T. Mori, T. Ogawa, D.C. Cho, and T. Mizutani, The 12th Int. Conf. on Solid Films and Surface, Marseille, France, 2002.
14. P.W.M. Blom, M.J.M. de Jong, and J.J.M. Vleggaar, Appl. Phys. Lett. **68** 3308 (1996).
15. S. Karg, M. Meier, and W. Riess, J. Appl. Phys. **82** 1951 (1997).
16. A.J. Cambell, D.D.C. Bradley, and D.G. Lidzey, J. Appl. Phys. **82** 6326 (1997).
17. J.C. deMello, N. Tessler, S.C. Graham, and R.H. Friend, Phys. Rev. B **57** 12951 (1998).
18. U. Wolf, S. Barth, and H. Bässler, Appl. Phys. Lett. **75** 2035 (1999).
19. T. Mori, E. Sugimura, and T. Mizutani, J. Phys. D: Appl. Phys. **26** 452 (1993).
20. K. Imaizumi, K. Kaneko, T. Mori, and T. Mizutani, 1999 Autum Meeting, Materials Research Society, Boston, USA (1999).

21. K. Imaizumi, K. Kaneko, T. Mori, and T. Mizutani, Int. Symp. on Oranic Molecular Electronics Proc. Nagoya, Japan, 2000.
22. K. Imaizumi, K. Kaneko, and T. Mori, T. Mizutani, The 10th Int. Work. on Inorganic & Organic. Electroluminescence, Hamamatsu, Japan, 2000.
23. K. Imaizumi, K. Kaneko, T. Mori, and T. Mizutani, Trans. IEE Jpn. **121-A** 332 (2001) [in Japanese].
24. K. Imaizumi, K. Kaneko, T. Mori, and T. Mizutani, Trans. IEE Jpn. **121-A** 666 (2001) [in Japanese].
25. K. Imaizumi, K. Kaneko, T. Mori, and T. Mizutani, Jpn. J. Appl. Phys. **41** 366 (2002).
26. T. Ogawa, D.-C. Cho, K. Kaneko, T. Mori, and T. Mizutani, IEICE Trans. Electron. **E85-C**, 1239 (2002).
27. D.V. Khramtchenkov, H. Bässler, and V.I. Arkhipov, J. Appl. Phys. **79** 9283 (1996).
28. P.S. Davids, I.H. Campbell, and D.L. Smith, J. Appl. Phys. **82** 6319 (1997).
29. B.K. Crone, P.S. Davids, I.H. Campbell, and D.L. Smith, J. Appl. Phys. **84** 833 (1998).
30. Y. Kawabe, M.M. Morrell, G.E. Jabbour, S.E. Shaheen, B. Kippelen, and N. Peyghambarian, J. Appl. Phys. **84** 5306 (1998).
31. G.G. Malliaras and J. Scott, J. Appl. Phys. **85** 7426 (1999).
32. J. Staudigel, M. Stöel, F. Steuber, and J. Simmerer, J. Appl. Phys. **86** 3895 (1999).
33. B.K. Crone, P.S. Davids, I.H. Campbell, D.L. Smith, C.J. Neef, and J. P. Ferraris, J. Appl. Phys. **86** 5767 (1999).
34. B.K. Crone, P.S. Davids, I.H. Campbell, and D.L. Smith, J. Appl. Phys. **87** 1974 (2000).
35. E. Tutis, M.N. Bussac, B. Masenelli, M. Carrad, and L. Zuppiroli, J. Appl. Phys. **89** 430 (2001).
36. T. Tsutsui, C.P. Lin, and S. Saito, Mol. Cryst. Liq. Cryst. **256** 63 (1994).
37. M. Iwamoto and T. Hino, Trans. IEE Jpn. A **100** 291 (1980) [in Japanese].